Electronic Supplementary Information for:

Reversible resistive switching behaviour in CVD grown, large area MoO$_x$

Fahmida Rahman[1*], Taimur Ahmed[1], Sumeet Walia[1], Edwin Mayes[2], Sharath Sriram[1], Madhu Bhaskaran[1] and Sivacarendran Balendhran[1*]

[1]Functional Materials and Microsystem Research Group and Micro Nano Research Facility, RMIT University, Melbourne, Victoria 3000 (Australia).
[2]RMIT Microscopy and Microanalysis Facility, RMIT University, Melbourne, Victoria 3000 (Australia).
Email: fahmida.rahman@gmail.com;shiva.balendhran@rmit.edu.au

S1. CVD growth temperature comparison

Table S1. A comparison of crystalline MoO$_3$ growth obtained via CVD, from various reports.

Authors	Growth temperature/°C	Pressure/mTorr	Phase of MoO$_3$	Reference
Kalantar-zadeh et al.	400	Ambient	α-MoO$_3$	S1
Balendhran et al.	350-560	Ambient	α-MoO$_3$	S2
Kim et al.(Plasma Enhanced CVD)	150	100	α-MoO$_3$	S3
Our work	530	300	α-MoO$_3$ /MoO$_2$	

S2. Pulse width and Energy consumption

To assess the cyclic endurance of the devices, a pulse train of width 2 ms was applied. A read pulse of 500 mV was applied after each SET and RESET pulse to measure the resistance of the device during LRS and HRS. The associated energies for SET and RESET switching were computed to be 6.7 μJ to 18 nJ range during the pulse switching.
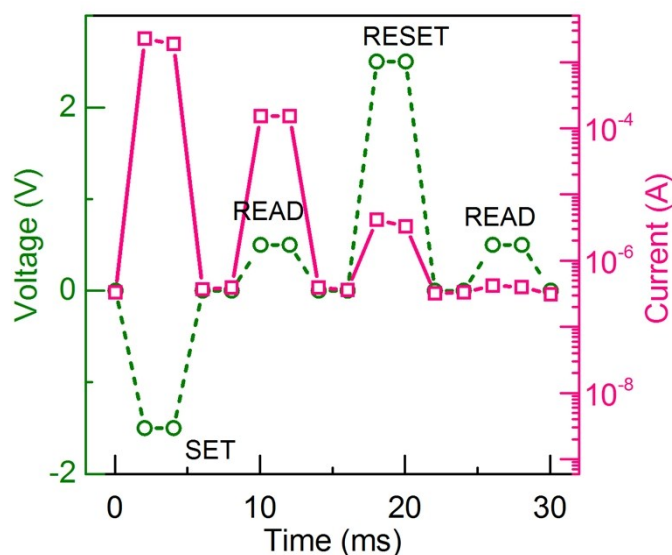
Fig. S1 A train pulse of width 2 ms was applied to measure the endurance of the device. Voltage *vs*. time and Current *vs*. time has been plotted to show the input and output curves.

S3. A quantitative performance comparison of various 2D materials

Table S2. Performance comparison of various 2D materials as resistive memory

Author	Material	ON/OFF ratio	Retention duration/s	endurance	References
Cheng et al.	MoS_2	10^3	---	1000	S4
Shin et al.	MoS_2	10^2	10^4	100	S5
Sangwan et al.	MoS_2	10^3	---	------	S6
Our work	MoO_x	10^3	10^4	>6000	

S4. Inverse FFT analysis of the cross-sectional TEM

In order to highlight the percentage of the crystalline area accurately, the TEM images of pristine and electroformed cells are sub-divided into smaller regions of interest (ROIs). Diffraction patterns corresponding to (001) plane of MoO_3 and (002) plane of MoO_2 are used to generate inverse fast Fourier transform (iFFT). The results are presented in Fig. S2 a and b, where the iFFT of pristine and electroformed cells are presented, respectively. The iFFT data is then analysed using ImageJ to determine the percentage crystalline area. The analysis indicates that the pristine film is composed of 72.50% of crystalline MoO_3 and MoO_2 while the remainder was observed to be amorphous in nature. After electroforming, 94.11% of the film was observed to be crystalline sub-stoichiometric MoO_3.
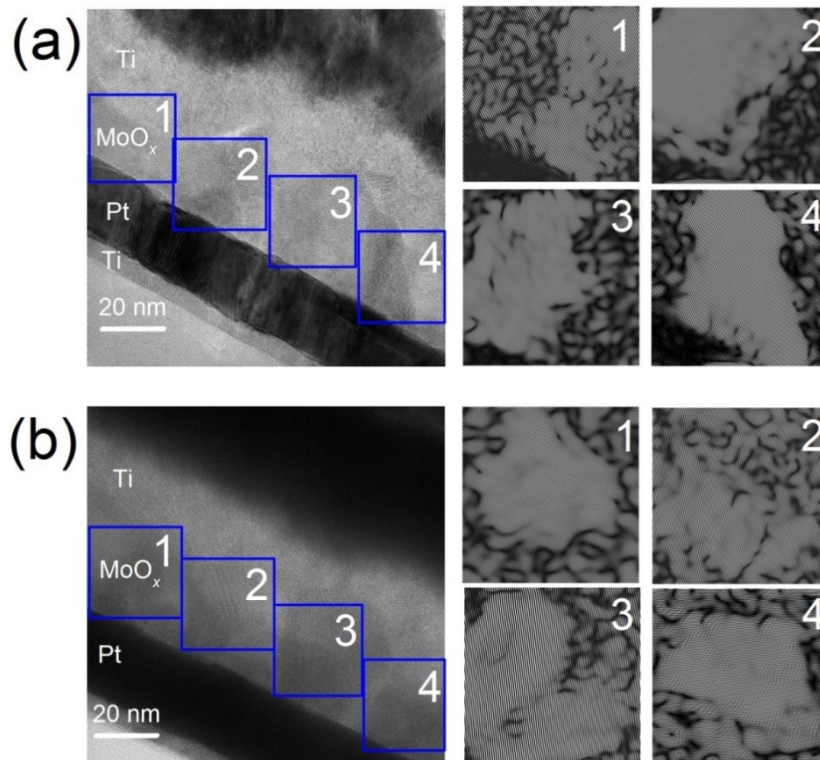
Fig. S2 HRTEM images of (a) a pristine cell and the corresponding iFFT of the ROIs numerically labelled from 1 to 4 and (b) an electroformed cell and the corresponding iFFT of the highlighted areas.

References

S1.   K. Kalantar-zadeh, J. Tang, M. Wang, K. L. Wang, A. Shailos, K. Galatsis, R. Kojima, V. Strong, A. Lech, W. Wlodarski and R. B. Kaner, *Nanoscale*, 2010, **2**, 429-433.

S2.   S. Balendhran, J. Deng, J. Z. Ou, S. Walia, J. Scott, J. Tang, K. L. Wang, M. R. Field, S. Russo, S. Zhuiykov, M. S. Strano, N. Medhekar, S. Sriram, M. Bhaskaran and K. Kalantar-Zadeh, *Adv. Mater.*, 2013, **25**, 109-114.

S3.   U. K. Hyeong, S. Juhyun, K. Atul, A. Chisung, K. Ki Seok, S. Dongjoo, Y. Geun Yong and K. Taesung, *Nanotechnology*, 2017, **28**, 175601.

S4.   P. Cheng, K. Sun and Y. H. Hu, *Nano Lett.*, 2016, **16**, 572-576.

S5.   S. Gwang Hyuk, K. Choong-Ki, B. Gyeong Sook, K. Jong Yun, J. Byung Chul, K. Beom Jun, W. Myung Hun, C. Yang-Kyu and C. Sung-Yool, *2D Mater.*, 2016, **3**, 034002.

S6.   V. K. Sangwan, D. Jariwala, I. S. Kim, K.-S. Chen, T. J. Marks, L. J. Lauhon and M. C. Hersam, *Nat. Nanotechnol.*, 2015, **10**, 403-406.